

Reionization and the large-scale 21 cm-cosmic microwave background cross correlation

Peter J. Adshead^{*} & Steven R. Furlanetto

Yale Center for Astronomy and Astrophysics, Yale University, PO Box 208121, New Haven, CT 06520-8121

1 February 2008

ABSTRACT

Of the many probes of reionization, the 21 cm line and the cosmic microwave background (CMB) are among the most effective. We examine how the cross-correlation of the 21 cm brightness and the CMB Doppler fluctuations on large angular scales can be used to study this epoch. We employ a new model of the growth of large scale fluctuations of the ionized fraction as reionization proceeds. We take into account the peculiar velocity field of baryons and show that its effect on the cross correlation can be interpreted as a mixing of Fourier modes. We find that the cross-correlation signal is strongly peaked toward the end of reionization and that the sign of the correlation should be positive because of the inhomogeneity inherent to reionization. The signal peaks at degree scales ($\ell \sim 100$) and comes almost entirely from large physical scales ($k \sim 10^{-2}$ Mpc). Since many of the foregrounds and noise that plague low frequency radio observations will not correlate with CMB measurements, the cross correlation might appear to provide a robust diagnostic of the cosmological origin of the 21 cm radiation around the epoch of reionization. Unfortunately, we show that these signals are actually only weakly correlated and that cosmic variance dominates the error budget of any attempted detection. We conclude that the detection of a cross-correlation peak at degree-size angular scales is unlikely even with ideal experiments.

Key words: cosmology: theory – cosmic microwave background – diffuse radiation

1 INTRODUCTION

During some epoch between recombination ($z \sim 1100$) and today, the intergalactic medium (IGM) underwent a transformation from almost completely neutral to almost completely ionized. When and how the IGM was ionized remains one of the most exciting open questions in cosmology (Barkana & Loeb 2001; Furlanetto et al. 2006). The timing and duration of this epoch of reionization contains a wealth of information about the first cosmic structures, information which is expected to help explain how the primordial density perturbations observed in the cosmic microwave background (CMB) evolved into the complex structures we observe in the low redshift universe today.

Currently there are only weak observational constraints on the epoch of reionization. The absence of a Gunn-Peterson trough in the spectra of $z < 6$ quasars indicates that reionization was complete by $z \sim 6$ (Fan et al. 2002; White et al. 2003; Fan et al. 2006), while integral constraints on the total optical depth from WMAP imply reionization began at $z \geq 10$ (Page et al. 2007; Spergel et al. 2006). A variety of other methods have been proposed, but none impose strong constraints (for recent summaries, see Fan et al. 2006 and Furlanetto et al. 2006).

The 21 cm hyperfine spin-flip transition of HI is the most exciting prospective tracer of the cosmic gas before and during reionization. This signal does not require the existence of bright background sources, which may be rare at high redshifts, making the entire epoch of reionization available (Scott & Rees 1990; Madau et al. 1997; Furlanetto et al. 2006). It is a line transition, so that observations at a given frequency select out a unique slice of the high z universe. Furthermore, fluctuations in the brightness of the 21 cm signal are caused by density (and ionization) inhomogeneities on all scales, making it a direct tracer of the underlying matter distribution (Zaldarriaga et al. 2004). Thus the spectral and angular variations of the 21 cm brightness allow us to reconstruct a 3D map of reionization. The epoch of reionization spans the formation of the first luminous sources, which then ionized the surrounding gas (Barkana & Loeb 2001). Thus a 3D map of the evolution of the neutral fraction and density field would provide an unprecedented view of this epoch of structure formation.

Ionization of the neutral IGM creates free electrons off of which CMB photons may be scattered. This Thomson scattering process has

^{*} peter.adshead@yale.edu

several effects (Hu et al. 1994; Dodelson & Jubas 1995). Photons from multiple lines of sight are blended together, damping the primary CMB anisotropies. The scattered photons also gain some of the peculiar momentum of the free electrons, generating a secondary anisotropy (most recently examined by Giannantonio & Crittenden 2007). Finally, the polarization dependence of Thomson scattering generates a new large scale polarization from the anisotropic CMB photon field (Zaldarriaga 1997).

Taken by itself, the CMB temperature provides only an integral constraint on the column density of ionized electrons, because the net damping is nearly independent of the location of the electrons. The induced polarization contains somewhat more information about the history of reionization, but it is difficult to extract even in a cosmic variance-limited survey (Holder et al. 2003; Mortonson & Hu 2007). Cross correlating with the 21 cm signal should allow more information to be extracted from both measurements. The cross correlation signal arises from the velocity field of ionized baryons, which sources the Doppler anisotropies in the CMB and also traces the linear overdensity of neutral hydrogen, the source of the 21 cm brightness. Alvarez et al. (2006) showed that combining the two measurements could in principle allow the extraction of the global reionization history, which is otherwise difficult to measure (e.g., Shaver et al. 1999; Furlanetto 2006). One reason is that the signal from the 21 cm radiation will be dominated by foregrounds and detector noise which makes extracting useful information difficult. Although many of these same foregrounds appear in the CMB, they are much smaller and more easily removed (and of course the thermal noise is uncorrelated). Cross-correlation with the CMB could therefore dramatically improve our confidence in the cosmological origin of the 21 cm signal.

This work is an improved calculation of results presented by Alvarez et al. (2006). In particular, we include the corrections to the 21 cm brightness due to redshift space distortions caused by the peculiar velocity field of neutral hydrogen (as in Bharadwaj & Ali 2004). We employ a more physically motivated reionization history together with a new model of the growth of the ionized contrast as reionization proceeds. We also re-examine the prospects for detecting the large scale cross-correlation. Unfortunately, we find that it will be extremely difficult because of cosmic variance. Throughout this work, we will confine the discussion to large angular scales (\sim degree) where the details of the the ionized bubbles that appear during reionization (Furlanetto et al. 2004a) largely average out. On smaller scales, these arcminute structures will also induce interesting cross-correlations (e.g., Cooray 2004; Salvaterra et al. 2005; Slosar et al. 2007), but the simple models based on linear theory used here will not suffice to describe them. Also, note that we will assume gaussian fluctuations throughout, as appropriate for linear matter fluctuations on the large scales we study. Only on smaller scales will higher-order correlations become important (Cooray 2004).

This paper is organized as follows. In §2 expressions for the 21 cm brightness, CMB Doppler brightness, and the cross-correlation signals are derived. Equation (22) is the main result. Section 3 details the reionization model, and §4 presents calculations of the observability of our predictions for future radio telescopes. Finally, we conclude in §5.

Throughout our work the following Fourier convention is used

$$f(\hat{\mathbf{n}}, \eta) = \int \frac{d^3\mathbf{k}}{(2\pi)^3} f_{\mathbf{k}} e^{-i\mathbf{k} \cdot \hat{\mathbf{n}}(\eta_0 - \eta)}. \quad (1)$$

The cosmological parameters are set at $\Omega_0 = 0.24$, $\Omega_b = 0.042$, $\Omega_\Lambda = 0.76$, $h = 0.73$, $\sigma_8 = 0.8$ and $n = 0.96$, consistent with the WMAP year three data (Spergel et al. 2006), and we use the matter power spectrum of Eisenstein & Hu (1997). We work in natural units where $c = 1$, so that in a flat geometry the conformal time,

$$\eta_0 - \eta(z) = \int_0^z \frac{dz'}{H(z')}, \quad (2)$$

equals the comoving distance, $r(z) = \eta_0 - \eta(z)$. Throughout $H(z)$ denotes the Hubble parameter. We will also use the expansion of the plane wave,

$$e^{-i\mathbf{k} \cdot \mathbf{x}} = \sum_{\ell=0}^{\infty} (-i)^\ell (2\ell+1) j_\ell(kx) \mathcal{P}_\ell(\hat{\mathbf{k}} \cdot \hat{\mathbf{x}}) \quad (3)$$

$$= 4\pi \sum_{\ell, m} (-i)^\ell j_\ell(kx) Y_{\ell m}(\hat{\mathbf{k}}) Y_{\ell m}^*(\hat{\mathbf{x}}), \quad (4)$$

where \mathcal{P}_ℓ is the Legendre polynomial of order ℓ .

2 21 CM AND CMB DOPPLER TEMPERATURE ANISOTROPY

2.1 21 cm Temperature Anisotropy

As long as the spin or excitation temperature, T_s , of the 21 cm transition in a region of the intergalactic medium (IGM) differs from the CMB temperature that region will appear in either emission ($T_s > T_{cmb}$) or absorption ($T_s < T_{cmb}$) when viewed against the CMB. Variations in the density of neutral hydrogen would appear as fluctuations in the sky brightness of this transition (Scott & Rees 1990; Madau et al. 1997; Furlanetto et al. 2006).

The optical depth of the IGM in the hyperfine transition is (Field 1958)

$$\tau_{21} = \frac{3c^3 \hbar A_{10} n_H}{16k_B \nu_0^2 T_s (1+z) (dv_r/dr)} x_{\text{HI}}, \quad (5)$$

where $A_{10} = 2.85 \times 10^{-15} \text{ s}^{-1}$ is the spontaneous emission coefficient, k_B is the Boltzmann constant, n_H is the number density of hydrogen, and x_{HI} is the neutral fraction. dv_r/dr is the gradient of the radial velocity along the line of sight, v_r being the physical velocity and r the comoving distance. This factor accounts for the bulk motion of the hydrogen, which causes a Doppler shift from the intrinsic line frequency, $\nu_0 = 1420.2 \text{ MHz}$.

Peculiar velocities induce a small perturbation in the gradient of the proper velocity away from the Hubble flow

$$\frac{dv_r}{dr} = a(z)H(z) + \frac{\partial v}{\partial r}, \quad (6)$$

where v is the radial peculiar velocity and $a(z)$ is the scale factor. To first order in the density perturbations the optical depth in the hyperfine transition is then

$$\tau_{21} \approx 8.6 \times 10^{-3} x_{\text{HI}} \left(1 + \delta_b(\hat{\mathbf{n}}, \eta) - \frac{1}{a(z)H(z)} \frac{\partial v_r}{\partial r} \right) \left[\frac{T_{\text{cmb}}(z)}{T_s} \right] \left(\frac{\Omega_b h^2}{0.02} \right) \left[\left(\frac{0.15}{\Omega_m h^2} \right) \left(\frac{1+z}{10} \right) \right]^{1/2}, \quad (7)$$

where $T_{\text{cmb}}(z) = 2.725(1+z) \text{ K}$ and we have assumed that the universe is matter-dominated at the redshifts of interest. In arriving at this expression we have neglected a number of terms, such as the effect of the CMB dipole in the gas frame and the local effects of gravitational redshifting, which also contribute to the 21 cm optical depth. However, these additional terms contribute less than 1% to the anisotropy on the scales of interest, and equation (7) suffices for our purposes (Lewis & Challinor 2007).

Following Zaldarriaga et al. (2004), we define $T_{21}(\hat{\mathbf{n}}, z)$ to be the observed brightness temperature increment between this patch and the CMB at an observed frequency ν corresponding to a redshift $1+z = \nu_0/\nu$ in a direction $\hat{\mathbf{n}}$,

$$T_{21}(z) \approx \frac{1}{1+z} (T_s - T_{\text{cmb}}) \tau_{21}, \quad (8)$$

where we have assumed that τ_{21} is small.

We now write the observed differential brightness temperature of the 21 cm emission line at $\lambda = 21 \text{ cm}(1+z)$ in the direction $\hat{\mathbf{n}}$ as

$$T_{21}(\hat{\mathbf{n}}, z) = T_0(z) \int_0^{\eta_0} d\eta' W[\eta(z) - \eta'] \psi_{21}(\hat{\mathbf{n}}, \eta'), \quad (9)$$

where $W[\eta(z) - \eta']$ is a normalized ($\int_{-\infty}^{\infty} dx W[x] = 1$) spectral response of an instrument which is centered at $\eta(z) - \eta' = 0$. $T_0(z)$ is a normalization factor given by

$$T_0(z) \simeq 23 \text{ mK} \left(\frac{\Omega_b h^2}{0.02} \right) \left[\left(\frac{0.15}{\Omega_m h^2} \right) \left(\frac{1+z}{10} \right) \right]^{1/2}, \quad (10)$$

and

$$\psi_{21}(\hat{\mathbf{n}}, \eta) \equiv x_{\text{HI}}(\hat{\mathbf{n}}, \eta) \left[1 + \delta_b(\hat{\mathbf{n}}, \eta) - \frac{1}{a(\eta)H(\eta)} \frac{\partial v_r}{\partial r} \right] \left[1 - \frac{T_{\text{cmb}}(\eta)}{T_s(\hat{\mathbf{n}}, \eta)} \right]. \quad (11)$$

We assume that the spectral resolution of the instrument is much smaller than the features of the target signal in redshift space. We thus set $W[x] = \delta^D(x)$, to obtain

$$T_{21}(\hat{\mathbf{n}}, z) = T_0(z) \psi_{21}[\hat{\mathbf{n}}, \eta(z)]. \quad (12)$$

On very small scales, this is a poor approximation because the finite bandwidth averages over many oscillations, damping the signal. However, for our regime of interest at $\ell \sim 100$ this is expected to be an excellent approximation (Zaldarriaga et al. 2004).

During most of reionization, we expect $T_s \gg T_{\text{cmb}}$ (Ciardi & Madau 2003; Furlanetto 2006), so we neglect the T_{cmb}/T_s term in equation (11). By writing the ionized fraction contrast

$$\delta_i \equiv \frac{x_i - \bar{x}_i}{\bar{x}_i}, \quad (13)$$

where x_i is the ionized fraction and the overbar denotes an average quantity, to first order in the density perturbations, equation (11) can be written

$$\psi_{21}(\hat{\mathbf{n}}, \eta) = \bar{x}_{\text{HI}} \left(1 + \delta_b(\hat{\mathbf{n}}, \eta) - \frac{1}{a(z)H(z)} \frac{\partial v_r}{\partial r} \right) - \bar{x}_i \delta_i(\hat{\mathbf{n}}, \eta). \quad (14)$$

It is important to note here that this is not necessarily a well-defined perturbation expansion. At any given point in space, the ionized fraction is either zero or unity, so that averaged over sufficiently small scales (of order the characteristic size of the HII regions), δ_i itself will be at least of order unity. However, we will only examine large scales ($\gg 10 \text{ Mpc}$) which average over many of these highly ionized regions, so equation (14) is acceptable.

Working in Fourier space, the baryon velocity field is related to the density contrast via the continuity equation, $\mathbf{v}_{\mathbf{k}} = -i\mathbf{k}/k^2 \dot{\delta}_{b,\mathbf{k}}(\eta)$, where the overdot denotes a derivative with respect to conformal time. At late times on the scales of interest, the perturbations scale as the

linear growth factor D_1 , so $\dot{\delta}_{b,k}(\eta) = \delta_{b,k} a(\eta) H(\eta) f$, where $f \equiv d \ln D_1 / d \ln a$ is the dimensionless linear growth rate or redshift space distortion factor (Kaiser 1987). Equation (14) becomes

$$\psi(\hat{\mathbf{n}}, \eta(z)) = \int \frac{d^3 k}{(2\pi)^3} \left[\bar{x}_{\text{HI}}(z) \delta_{\mathbf{k}}(z) \left(1 - \frac{f}{k^2} \frac{\partial^2}{\partial \eta^2} \right) - \bar{x}_i(z) \delta_{i\mathbf{k}}(z) \right] e^{ik\mu\eta}. \quad (15)$$

The multipoles of the spherical harmonic expansion are then

$$a_{\ell m}^{21}(z) = 4\pi(-i)^\ell T_0(z) \int \frac{d^3 k}{(2\pi)^3} \{ \bar{x}_{\text{HI}}(z) \delta_{\mathbf{k}}(z) J_\ell[k(\eta_0 - \eta(z))] - \bar{x}_i(z) \delta_{i\mathbf{k}}(z) j_\ell[k(\eta_0 - \eta(z))] \} Y_{\ell m}^*(\hat{\mathbf{k}}). \quad (16)$$

where (Bharadwaj & Ali 2004; Barkana & Loeb 2005),

$$J_\ell(x) = -f \frac{\ell(\ell-1)}{4\ell^2-1} j_{\ell-2}[k(\eta_0 - \eta(z))] + \left(f \frac{(2\ell^2+2\ell-1)}{4\ell^2+4\ell-3} + 1 \right) j_\ell[k(\eta_0 - \eta(z))] - f \frac{(\ell+2)(\ell+1)}{(2\ell+1)(2\ell+3)} j_{\ell+2}[k(\eta_0 - \eta(z))], \quad (17)$$

although we also include the redshift space distortion factor f . This is well approximated by $f = \Omega_m^{0.6}$, which for the redshifts of interest is approximately one. Neglecting the peculiar velocity perturbations amounts to taking $J_\ell(x) \rightarrow j_\ell(x)$.

To this point, our calculation is similar to that of Alvarez et al. (2006), except that we have incorporated the velocity correction in a different manner. They differentiated the plane wave before expanding in spherical coordinates. This left a factor $(1+\mu^2)$, where $\mu = \hat{\mathbf{n}} \cdot \mathbf{k}/|\mathbf{k}|$ is the angle between the line of sight direction $\hat{\mathbf{n}}$ and the photon propagation vector \mathbf{k} . On the other hand, we expand the plane wave into a spherical basis before taking the derivative. Both approaches are mathematically equivalent, but the advantage of ours will become apparent when calculating the cross-correlation.

2.2 The CMB Doppler Signal

In Fourier space, the secondary CMB temperature anisotropy from the Doppler effect is given by the line of sight integral

$$T_D(\hat{\mathbf{n}}, \mathbf{k}) = -T_{\text{cmb}} \int_0^{\eta_0} d\eta (-\dot{\tau}) \mu v_{b\mathbf{k}} e^{ik\mu(\eta-\eta_0)} e^{-\tau} = -T_{\text{cmb}} \int_0^{\eta_0} d\eta (-\dot{\tau}) e^{-\tau} \frac{v_{b\mathbf{k}}}{ik} \frac{\partial}{\partial \eta} [e^{ik\mu(\eta-\eta_0)}]. \quad (18)$$

We define $\tau(\eta) = \int_\eta^{\eta_0} d\eta \sigma_T n_e a$ so that $\dot{\tau} = -\sigma_T n_e a$. Note that with this definition $(-\dot{\tau}) > 0$.

As above, the baryon velocity field is related to the density contrast via the continuity equation. Thus in real space, assuming an observer positioned at the present day ($\eta = \eta_0$), we have

$$T_D(\hat{\mathbf{n}}) = T_{\text{cmb}} \int_0^{\eta_0} d\eta \dot{D}(-\dot{\tau}) e^{-\tau} \int \frac{d^3 k}{(2\pi)^3} \frac{\delta_{\mathbf{k}}}{k^2} \frac{\partial}{\partial \eta} e^{-ik\mu(\eta_0-\eta)}. \quad (19)$$

Expanding in spherical coordinates, the multipole moments are

$$a_{\ell m}^D = 4\pi T_{\text{cmb}} (-i)^\ell \int_0^{\eta_0} d\eta \dot{D}(-\dot{\tau}) e^{-\tau} \int \frac{d^3 k}{(2\pi)^3} \frac{\delta_{\mathbf{k}}}{k^2} \left[\frac{\partial}{\partial \eta} j_\ell[k(\eta_0 - \eta)] \right] Y_{\ell m}^*(\hat{\mathbf{k}}). \quad (20)$$

2.3 Doppler-21 cm Cross Correlation

We now calculate the cross correlation power spectrum, $C_\ell^{21-D} = \langle a_{\ell m}^{21} a_{\ell m}^{D*} \rangle$. We define the 3D power spectrum, $\langle \delta_{\mathbf{k}}(z) \delta_{\mathbf{k}'}(z) \rangle = (2\pi)^3 \delta^D(\mathbf{k} - \mathbf{k}') P_{\delta\delta}(k, z)$ and the cross-correlation power spectrum between the ionized fraction and density, $\langle \delta_{\mathbf{k}}(z) \delta_{i,\mathbf{k}'}(z) \rangle = (2\pi)^3 \delta^D(\mathbf{k} - \mathbf{k}') P_{\delta i}(k, z)$. We have

$$\begin{aligned} \langle a_{\ell m}^{21}(z) a_{\ell m}^{D*} \rangle &= -T_0(z) T_{\text{cmb}} \frac{2D_1(z)}{\pi} \int dk [\bar{x}_{\text{HI}}(z) P_{\delta\delta}(k) J_\ell[k(\eta_0 - \eta(z))] \\ &\quad - \bar{x}_i(z) P_{\delta i}(k) j_\ell[k(\eta_0 - \eta(z))]] \int_0^{\eta_0} d\eta' \dot{D}_1(-\dot{\tau}) e^{-\tau} \frac{\partial}{\partial \eta'} j_\ell[k(\eta_0 - \eta')]. \end{aligned} \quad (21)$$

We perform an integration by parts, and neglect the surface term since at early times $\tau \approx \infty$ and at late times $\dot{\tau}(0)$, the scattering rate, is essentially zero. We obtain

$$\begin{aligned} \langle a_{\ell m}^{21}(z) a_{\ell m}^{D*} \rangle &= -T_0(z) T_{\text{cmb}} \frac{2D_1(z)}{\pi} \int_0^{\eta_0} d\eta' \frac{\partial}{\partial \eta'} [\dot{D}_1(-\dot{\tau}) e^{-\tau}] \int dk j_\ell[k(\eta_0 - \eta')] \\ &\quad \times \{ \bar{x}_{\text{HI}}(z) P_{\delta\delta}(k) J_\ell[k(\eta_0 - \eta(z))] - \bar{x}_i(z) P_{\delta i}(k) j_\ell[k(\eta_0 - \eta(z))] \}. \end{aligned} \quad (22)$$

Compared to the expression of Alvarez et al. (2006), we have the factor $J_\ell[k(\eta_0 - \eta(z))]$ instead of $4/3 j_\ell[k(\eta_0 - \eta(z))]$. To obtain equation (22), we have simply required the orthogonality of the spherical harmonics to evaluate $\int d\Omega Y_\ell(\mu, \phi) Y_{\ell'}^*(\mu, \phi)$. However, if the factor μ^2 is included instead, as in Alvarez et al. (2006), then one must evaluate $\int d\Omega \mathcal{P}_2(\mu) Y_\ell(\mu, \phi) Y_{\ell'}^*(\mu, \phi)$, where $\mathcal{P}_2(\mu)$ is the second Legendre polynomial. Alvarez et al. (2006) approximated this integral with its value for $\ell = 0$, introducing the factor $4/3$.

Ignoring the velocity corrections to the 21 cm signal for a moment [this amounts to taking $J_\ell(x) \rightarrow j_\ell(x)$], and using the Limber approximation (proved in appendix A):

$$\frac{2}{\pi} \int_0^\infty k^2 dk \frac{P(k)}{k^2} j_\ell(kr) j_\ell(kr') \approx P\left(k = \frac{\ell}{r}\right) \frac{\delta(r-r')}{\ell^2}, \quad (23)$$

valid for $\ell \gg 1$, yields

$$\frac{\ell^2 C_\ell^{21-D}}{2\pi} = T_0(z) T_{cmb} \frac{D_1(z)}{2\pi} \frac{\partial}{\partial \eta} (\dot{D}_1 \dot{\tau} e^{-\tau}) \left[\bar{x}_{HI}(z) P_{\delta\delta} \left(\frac{\ell}{r(z)} \right) - \bar{x}_i(z) P_{i\delta} \left(\frac{\ell}{r(z)} \right) \right]. \quad (24)$$

This form is identical to equation (17) of Alvarez et al. (2006), except without their factor of 4/3. It follows from equation (24) that the cross correlation power spectrum should roughly trace the shape of the underlying matter power spectrum (at least for uniform reionization, or for $\delta_i \propto \delta$ as below). The matter power spectrum has a broad peak on the scale of the horizon size at matter-radiation equality, $k_{eq} \simeq 0.009 \text{ Mpc}^{-1} (\Omega_m h^2 / 0.128)$. Using the fact the the conformal time is on the order of 10^4 Mpc for large z , equation (24) implies that the cross correlation power spectrum will have a peak at degrees scales or $\ell \sim kr \sim 100$. For the rest of the paper we take $\ell_{peak} = 100$.

Equation (24) implies another important fact: there is a one-to-one correspondence between k and ℓ , so each multipole samples only one scale. In the exact case this is only approximately true; the right hand side of equation (23) is not a true delta function but has some finite width, which means that modes are mixed. The peculiar velocity corrections further mix the modes as seen through the appearance of $j_{\ell+2}(kx)$ and $j_{\ell-2}(kx)$ in equation (17). These redshift space distortions boost the signal by about 20% at ℓ_{peak} .

To obtain a numerical result we need a sensible model for the reionization history. On the scales of interest, density perturbations grow linearly. We therefore use a growth factor normalized so that $D_1(z_N) = 1$, or

$$\dot{D}_1 = -H(z) \frac{d}{dz} \left(\frac{1+z_N}{1+z} \right). \quad (25)$$

Assuming that only hydrogen is ionized,

$$\begin{aligned} -\dot{\tau} &= \frac{\sigma_T \rho_{b0}}{m_p} (1 - Y_p) (1+z)^2 \bar{x}_i(z) \\ &= 0.0525 H_0 \Omega_b h (1+z)^2 \bar{x}_i(z), \end{aligned} \quad (26)$$

where $Y_p = 0.24$ is the helium mass abundance. Taking $e^{-\tau} \approx 1$, since $\tau \sim 0.1$ (Spergel et al. 2006), then gives (Alvarez et al. 2006):

$$\frac{\partial}{\partial \eta} [\dot{D}_1 (-\dot{\tau}) e^{-\tau}] = -0.0525 H_0 \Omega_b h (1+z_N) H(z) \frac{d}{dz} [\bar{x}_i(z) H(z)]. \quad (27)$$

The combination $(1+z_N)^2 P(k, z_N)$ leaves equations (22) and (24) independent of the epoch of normalization z_N (Hu 1996).

As noted above, the shape of the cross correlation power spectrum for fixed z is determined entirely by the underlying matter power spectrum. For fixed ℓ its variation with redshift is determined primarily by the quantity $\partial/\partial \eta (\dot{D}_1 \dot{\tau} e^{-\tau})$, which from equation (27) depends on $d/dz [\bar{x}_i(z) H(z)]$. This implies another important fact: the cross-correlation vanishes when $d/dz [\bar{x}_i(z) H(z)]$ is constant and will be the largest where $[\bar{x}_i(z) H(z)]$ has the greatest rate of change. Models with faster rates of reionization and reionization occurring at higher redshifts will lead to larger cross-correlations (see below). This behavior comes directly from the CMB Doppler signal; unless the ionized fraction is changing, the line of sight integral in equation (19) suffers severe cancelation due to the oscillatory nature of the Bessel functions. Furthermore, this means that if dilution from the Hubble expansion is faster than the reionization rate, then the CMB will be on average blueshifted by reionization (and vice versa). During reionization \bar{x}_i will almost definitely be increasing very rapidly, so redshifting will be the dominant effect.

To get an idea of how the velocity corrections affect the signal we chose a simple parametrization of the neutral fraction to compare with previous results (Furlanetto et al. 2004b; Alvarez et al. 2006);

$$\bar{x}_{HI}(z) = \frac{1}{1 + \exp[-(z - z_r)/\Delta z]}, \quad (28)$$

Figure 1 shows the cross-correlation at $z = 15$ for homogeneous reionization ($P_{\delta i} = 0$) using equation (28) with $\Delta z = 1$ and $z_r = 15$. The three curves show the Limber approximation of equation (23), the exact result, and the anisotropy ignoring velocity corrections (i.e., $J_\ell \rightarrow j_\ell$), from top to bottom. Note how the Limber approximation works extremely well at $\ell \gg 100$ but overestimates the signal by $\sim 10\%$ near ℓ_{peak} and fares considerably worse at small ℓ . Velocities boost the signal on large angular scale by tens of percent but become unimportant on small scales. Note that the result of Alvarez et al. (2006) corresponds to 4/3 times the lower curve, which at $\ell \sim 100$ is not a bad approximation but gets worse as ℓ increases.

2.4 The Cross-Correlation Coefficient

We will find later on that it is convenient to re-cast many of our results in terms of the cross-correlation coefficient r ,

$$C_\ell^{21-D} = r \sqrt{C_\ell^{21} C_\ell^{CMB}}, \quad (29)$$

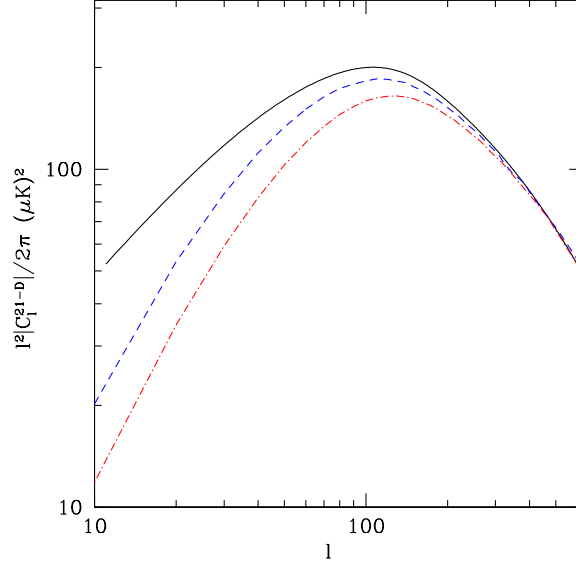


Figure 1. Cross-correlation angular power spectrum. The solid curve is calculated using the Limber approximation. The dot-dashed curve is the exact numerical integration without the velocity corrections and the dashed curve includes the velocity corrections. We take $z_r = 15$, $\Delta z = 1$, and $z = 15$

where C_ℓ^{21} is the angular power spectrum of the 21 cm signal and C_ℓ^{CMB} is the angular power spectrum of the CMB; in particular, we are interested in the Doppler contribution to the latter, C_ℓ^{DD} . The *maximal* cross-correlation coefficient will be $r_{\max} = \sqrt{C_\ell^{DD}/C_\ell^{CMB}}$, because the 21 cm signal is (nearly) uncorrelated with the primordial CMB anisotropy and other secondaries.

We can estimate the intrinsic 21 cm signal with a little bit of work from equation (16). Neglecting redshift space distortions, which give about a 30% correction at $\ell = 100$, and using the results above, we have (Zaldarriaga et al. 2004)

$$C_\ell^{21}(z) = (4\pi)^2 T_0(z)^2 \int k^2 \frac{dk}{(2\pi)^3} j_\ell[k(\eta_0 - \eta(z))]^2 [\bar{x}_{\text{HI}}^2 P(k, z) + \bar{x}_i^2 P_{ii}(k, z) - 2\bar{x}_{\text{HI}}\bar{x}_i P_{\delta i}(k, z)], \quad (30)$$

where P_{ii} is the power spectrum of δ_i .

We can estimate the CMB power from the Doppler signal from equation (20),

$$\langle a_{\ell,m}^D a_{\ell,m}^{D*} \rangle = T_{\text{cmb}}^2 \int_0^{\eta_0} d\eta \frac{\partial}{\partial \eta} [\dot{D}(-\dot{\tau})e^{-\tau}] \int_0^{\eta_0} d\eta' \frac{\partial}{\partial \eta'} [\dot{D}(-\dot{\tau}')e^{-\tau'}] \frac{2}{\pi} \int dk P(k) j_\ell[k(\eta_0 - \eta)] j_\ell[k(\eta_0 - \eta')], \quad (31)$$

where we have used the orthogonality of the spherical harmonics and integrated by parts twice. Using the Limber approximation (eq. 24), we obtain

$$\frac{\ell^2 C_\ell^{DD}}{2\pi} = \frac{T_{\text{cmb}}^2}{2\pi \ell^2} \int_0^{\eta_0} d\eta \left(\frac{\partial}{\partial \eta} [\dot{D}(-\dot{\tau})e^{-\tau}] \right)^2 P\left(\frac{\ell}{r(\eta)}\right) (\eta_0 - \eta)^2. \quad (32)$$

Note that the amplitude of this expression is primarily determined by the factor $\partial/\partial\eta(\dot{D}\dot{\tau}e^{-\tau})$, which as we saw above depends on $d/dz[\bar{x}_i(z)H(z)]$; the Doppler signal will be largest for models of reionization which occur at high redshifts and which proceed quickly.

3 THE REIONIZATION HISTORY

The prescription of equation (28) is not a well-motivated model of reionization. The quantity of interest for the cross-correlation, the rate at which the ionized fraction is changing, is completely determined by the free parameter Δz , so the form has no predictive power. Moreover, as soon as the ionized fraction reaches 1/2, the rate of reionization begins to slow, so the *shape* of the signal is prescribed “by hand” rather than following from physically-motivated arguments (e.g., recombinations). Our next task is therefore to estimate the signal on more physically-satisfying grounds.

However, in this paper we do not aim to present a complete model of reionization. Instead we will use a simple model that encapsulates many of the basic features in the global evolution. We begin by assuming that a galaxy of mass m_{gal} can ionize a mass ζm_{gal} , where ζ is the ionizing efficiency: a measure of the number of ionizing photons produced per baryon inside galaxies. This amounts to the assumption of an “inside-out” reionization scenario wherein the gas is first ionized by galaxies within overdense regions. This is consistent with numerical simulations, at least when the sources resemble star forming galaxies (McQuinn et al. 2005). We then associate the reionization rate with the star formation rate (Furlanetto 2006);

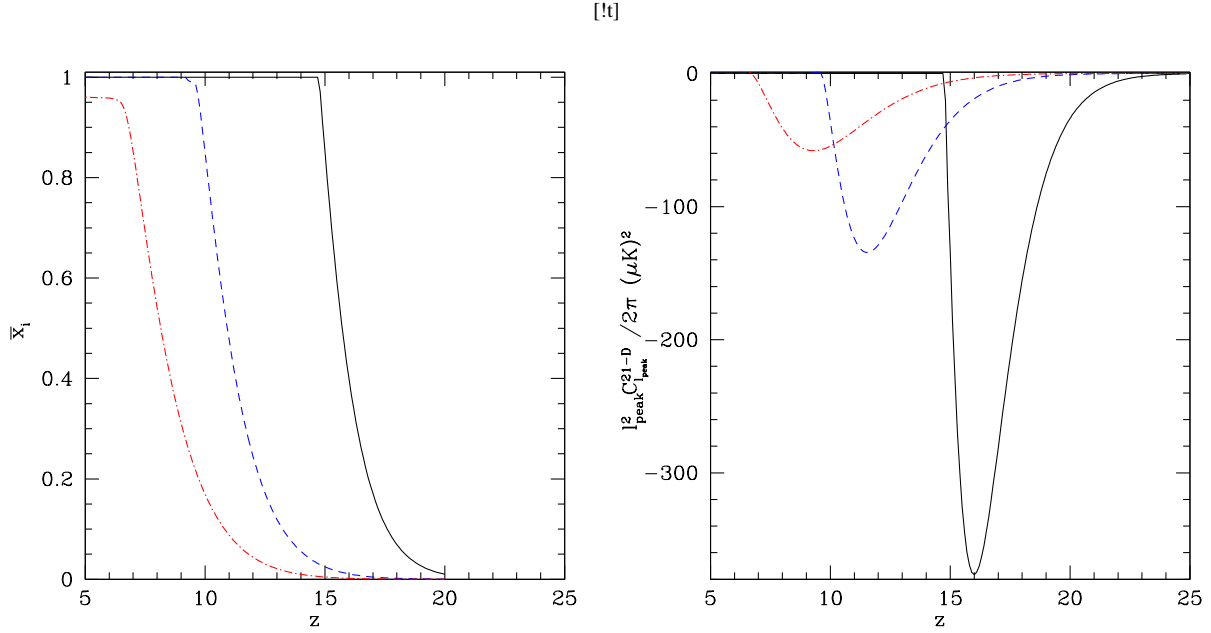


Figure 2. *Left panel:* The reionization model of Furlanetto (2006) with $\bar{x}_i \approx 1$ at $z=7$ (dot-dashed curve), 10 (dashed curve) and 15 (solid curve). *Right panel:* The contribution of the homogeneous term to the signal at ℓ_{peak} for the same models.

$$\frac{d\bar{x}_i}{dt} = \zeta \frac{df_{\text{coll}}}{dt} - \alpha_A C(z, \bar{x}_i) \bar{x}_i(z) \bar{n}_e(z), \quad (33)$$

where f_{coll} is the mass bound to halos above some mass threshold m_{min} . In this work we take the minimum mass to correspond to a virial temperature of 10^4 K (Barkana & Loeb 2001) and use the Press & Schechter (1974) mass function for simplicity. The second term on the right acts as a sink describing recombinations. $\alpha_A = 4.2 \times 10^{-12} \text{ cm}^3 \text{ s}^{-1}$ is the case-A recombination coefficient at 10^4 K, $C \equiv \langle n_e^2 \rangle / \langle n_e \rangle^2$ is the clumping factor for ionized gas, and \bar{n}_e is the average electron density in ionized regions.

The physics underlying the ionization efficiency is highly uncertain and depends on poorly understood intra-galactic dynamics, so in this work we take it as a free parameter. In principle ζ and m_{min} could vary with redshift due to feedback mechanisms. In most cases, feedback decreases ζ , and hence the reionization rate. Thus in models that include feedback, we expect the cross-correlation to be smaller and the peak to occur earlier in the ionization history (e.g. Furlanetto & Loeb 2005). For example, if the photoheating that accompanies reionization suppressed star formation in small galaxies, ζ would decrease significantly once $\bar{x}_i \gtrsim 0.5$, stretching reionization over a longer time interval (possibly enough to create an inflection point in the history; see below). In extreme cases, where recombinations dominate early in reionization, there could even be a turnover in \bar{x}_i (Cen 2003; Wyithe & Loeb 2003), which would strongly affect the cross-correlation (Alvarez et al. 2006).

The clumping factor, C , can in principle be computed with numerical simulations that incorporate radiative transfer. However, this requires fully resolving small scale structure in the IGM as well as tracking its evolution through reionization. Furthermore, C depends on how the IGM was ionized; whether low density gas was ionized first or if many photons were consumed ionizing dense blobs when \bar{x}_i was small (Furlanetto & Oh 2005). This means that C must be recomputed for each different set of model parameters. Simulations have unfortunately not yet reached these goals. We instead use a simple analytic model (Miralda-Escude et al. 2000) in which voids are ionized first.¹ This model perhaps underestimates the mean recombination rate, and so reionization probably proceeds a little slower than the model predicts. This means that our models will overestimate the signal and will predict a peak that is slightly later. This optimistic assumption about the speed of reionization means that our conclusions about the difficulty in observability of the signal should be robust to uncertainties in the history of reionization.

The left panel of Figure 2 shows the ionized fraction as a function of redshift for three scenarios, with reionization finishing by $z = 15$, $z = 10$ and $z = 7$. They have CMB optical depths of $\tau = 0.17$, 0.10, and 0.06 respectively.

We are now in a position to calculate the cross correlation under the assumption that reionization is uniform ($\delta_i = 0$ everywhere). In this case $P_{\delta_i}(k) = 0$ and only the first term in equation (22) contributes. The right panel of Figure 2 shows $\ell^2 C_{\ell}^{21-D} / 2\pi$ for the reionization models described above. We show its value as a function of redshift at ℓ_{peak} ; the shape of the angular spectrum is only weakly dependent

¹ This may at first seem to conflict with our assumption that ionization begins in dense environments. In fact, the ionizing photons will begin in large-scale overdense regions, but within the resulting ionized bubbles they will tend to ionize the low-density gas first. As a result, the Miralda-Escude et al. (2000) model underpredicts the recombination rate by a factor of a few early in reionization (Furlanetto & Oh 2005), but that has little effect on our results.

on redshift. Each curve corresponds to the matching reionization history on the left. The signal is negative (implying an anti-correlation) and peaks where the ionized fraction is changing the fastest. The signal decreases toward lower redshifts for three reasons. First and most importantly, the Hubble expansion dilutes the electron densities and hence decreases the scattering rate of CMB photons. Second, $\dot{f}_{\text{coll}}/f_{\text{coll}}$ decreases with cosmic time (though only gently), so the relative ionization rate decreases somewhat in scenarios with late reionization. Finally, the clumping factor C also increases with cosmic time, slowing the tail end of reionization most severely when z_r is small.

Alvarez et al. (2006) also used a physically-motivated model for the ionization history that included both galaxy collapse and recombinations. The major difference with our model is that they prescribed $\bar{x}_i(z)$ to have a particular functional form that matches smoothly onto $\bar{x}_i = 1$ (something that we achieve with a dynamically evolving clumping factor). Comparing their Fig. 3 with the $z = 15$ curve in our Figure 2, we predict a larger signal that peaks later in the reionization history. This follows directly from the different reionization histories: the functional form prescribed by Alvarez et al. (2006) has an inflection point where $\bar{x}_i = 1/2$, which causes their estimate to peak slightly earlier. As noted above, such a feature could arise in our model from feedback. Our amplitude is also larger because $\dot{f}_{\text{coll}}/f_{\text{coll}}$ is large throughout that epoch; again, the smooth functional form prescribed by Alvarez et al. (2006) suppressed this dependence but may be more realistic in the presence of strong feedback.

3.1 Inhomogeneous Reionization

Reionization is expected to be inhomogeneous for two reasons: the clumpiness of the IGM and the clustering of the discrete ionizing sources. The density-ionization cross correlation P_{δ_i} is a measure of this inhomogeneity. Given that little is known about the epoch of reionization and that many of the parameters describing the evolution are completely unconstrained, it is difficult to construct detailed models for this correlation. We will therefore rely on the simplest approach that we can.

To calculate this correlation we need a model of how the perturbations to the ionized contrast δ_i grow through reionization. Ideally we want to relate these to the underlying matter overdensity δ so that we can express P_{δ_i} in terms of $P_{\delta\delta}$. One potential problem is that, on small scales, fully ionized bubbles can have $\delta_i \gg 1$. Fortunately, on large scales these bubbles average out so that linear theory will suffice in the regime of interest.

As before, we assume reionization proceeds “inside-out” so that a galaxy of mass m_{gal} can ionize a bubble of mass ζm_{gal} around it. It follows that, for an isolated large region of overdensity δ (Furlanetto et al. 2004a),

$$x_i(\delta) = \bar{x}_i(1 + \delta_i) = \zeta f_{\text{coll}}(\delta), \quad (34)$$

where $f_{\text{coll}}(\delta)$ is the conditional collapsed fraction in our region. Note that the assumption of an *isolated* region is key here. It is adequate on the large, $\gtrsim 100$ Mpc scales we are interested in because ionizing photons are never able to travel such large distances during reionization (Furlanetto et al. 2004a). A model like that above fails if applied on ~ 10 Mpc scales, because photons from sources outside the region become relevant. Expanding this to linear order, we have $f_{\text{coll}}(\delta) = f_{\text{coll}}(1 + \bar{b}\delta)$. Here \bar{b} is the mean galaxy bias (averaged over all galaxies; Mo & White 1996). For an individual galaxy of mass m , the Press & Schechter (1974) mass function yields

$$b(m) = \left[1 + \frac{\delta_c}{\sigma(m)^2 D_1(z)} - \frac{1}{\delta_c(z) D_1(z)} \right], \quad (35)$$

where δ_c is the critical density for spherical collapse and $\sigma^2(m)$ is the fractional variance of the density field when smoothed on spheres of mass m . The average over all galaxies is

$$\bar{b} = \frac{1}{f_{\text{coll}}} \int dm \frac{m}{\bar{\rho}} n(m) b(m). \quad (36)$$

Note that the same expression follows from the reionization model of Furlanetto et al. (2004a) by integrating over the galaxy population of each ionized bubble in a large-scale region of overdensity δ . We show the mean bias as a function of redshift in the upper left panel of Figure 3.

In this model, we therefore have $\delta_i = \bar{b}\delta$. Before proceeding further, we must address two more potential problems with our approach. The condition that the ionized fraction everywhere be less than unity implies

$$1 \geq x_i = \bar{x}_i(1 + \bar{b}\delta), \quad (37)$$

which can be written

$$\bar{b}\delta \leq \frac{1 - \bar{x}_i}{\bar{x}_i}. \quad (38)$$

On the scales of interest we can estimate $\delta \sim \sigma(R)$. $\ell = 100$ corresponds to $R \sim 200$ Mpc, where $\sigma(200 \text{ Mpc}, z = 10) \sim 0.004$. We are interested in the epoch in which $\bar{x}_i \sim 0.5$; so \bar{b} can be as large as ~ 360 and our approximations will still remain valid.

This prescription poses one final problem: as reionization proceeds, the ionized contrast grows monotonically with the bias, irrespective of the ionized fraction. This ignores two subtleties of reionization. First, even on these large scales the ionized features will eventually grow large enough that the regions are no longer independent (i.e., low-density voids will eventually be ionized by their neighbors). Moreover, Furlanetto & Oh (2005) have shown that recombinations become important for larger bubbles. They imprint a maximum size R_{max} on

reionized regions; any extra photons produced in these bubbles are canceled out by recombinations. Although this process is difficult to model in detail (especially given the weak constraints on structure in the IGM at high redshift), we can approximately account for these effects by modifying δ_i to

$$\delta_i = \bar{b}\delta(1 - f_{\text{sat}}), \quad (39)$$

where f_{sat} is the fraction of the volume in the “saturated” bubbles (with $R > R_{\text{max}}$). As \bar{x}_i approaches unity, so must f_{sat} , so the effective bias $\bar{b}(1 - f_{\text{sat}})$ eventually goes to zero. In other words, we subtract off photons produced inside regions where recombinations dominate, because they are consumed before helping to ionize new material. Unfortunately R_{max} depends sensitively on the distribution of high-redshift Lyman-limit systems, whose origins are uncertain. There is thus no particularly good model for R_{max} or f_{sat} . However, the curves in Fig. 10 of Furlanetto & Oh (2005) are reasonably well-described by

$$f_{\text{sat}}(\bar{x}_i) = \exp\left[\frac{|\bar{x}_i - 1|}{\Delta\bar{x}_i}\right], \quad (40)$$

where $\Delta\bar{x}_i$ is a parameter which encodes the effects of the recombining bubbles (which increases as R_{max} decreases, because the saturation limit is reached earlier for smaller bubbles). The upper right panel of Fig. 3 shows f_{sat} for $\Delta\bar{x}_i = 0.2, 0.1$, and 0.05 . These values of $\Delta\bar{x}_i$ are chosen to roughly match the results of Furlanetto & Oh (2005) and correspond to $z = 6, z = 9$, and $z = 12$ respectively (with recombinations setting in earlier at lower redshifts because the clumpiness C increases with time).

Finally, the density-ionization cross correlation power spectrum is given by:

$$\begin{aligned} P_{i\delta}(k, z) = \langle \delta_{i\mathbf{k}}(z) \delta_{\mathbf{k}'}(z) \rangle &= \bar{b}(z)(1 - f_{\text{sat}}) \langle \delta_{\mathbf{k}}(z) \delta_{\mathbf{k}'}(z) \rangle \\ &= \bar{b}(z)(1 - f_{\text{sat}}) P(k, z). \end{aligned} \quad (41)$$

Current simulations do not have large enough box sizes to test this approximation on the $\gtrsim 100$ Mpc scales of interest. However, on the largest scales that we can compare ($k \sim 0.1 \text{ Mpc}^{-1}$), our result is $\sim 10\%$ larger than that obtained from “semi-numerical” simulations of the reionization process, at least early in reionization (Mesinger & Furlanetto 2007). As reionization proceeds, the simulations show that the amplitude on this scale gets even larger; this is because the characteristic size of ionized bubbles reaches $k \sim 0.1 \text{ Mpc}^{-1}$ about midway through the process. We do not expect such an amplification to occur at the scales relevant to the cross-correlation so long as the bubbles do not reach such large sizes.

The lower panels of Figure 3 show the variation in redshift space of the cross-correlation signal, with the left panel showing the individual contributions of the homogeneous and inhomogeneous terms and the right panel showing the sum. For reference, $z = 7, 10$ and 15 correspond to $\nu = 177.5, 129.1$ and 88.8 MHz respectively.

The bottom left panel of Figure 3 shows that the positively correlated inhomogeneous part of the signal strongly dominates over the anti-correlated homogeneous part. This is because the inhomogeneous component is so strongly biased (upper left panel). Its amplitude increases rapidly with redshift for two reasons: the quantity $d/dz[H(z)\bar{x}_i(z)]$ is larger for earlier reionization and the galaxy bias grows large at higher redshifts (see the upper left panel of Fig. 3). Our amplitudes are somewhat larger than those of Alvarez et al. (2006) because our reionization models allow larger $d\bar{x}_i/dz$ and because our cosmology yields larger bias factors at high redshift.

In the lower right panel we explore the effects of varying the rate at which bubbles saturate by varying the parameter $\Delta\bar{x}_i$. If saturation sets in earlier the peak amplitude of the signal decreases, and the peak also moves earlier in reionization. However, in all of these cases f_{sat} has little effect except in a brief redshift interval. This is simply because \bar{x}_i increases from ~ 0.5 to ~ 1 so quickly. We find, therefore, that measuring the peak amplitude of the cross correlation does not precisely yield the rate at which reionization is occurring (or, in our simple model, roughly the rate at which gas collapses onto galaxies); rather, it provides the rate at which photons are able to escape from the environs of their source galaxy. Late in reionization, the overall amplitude will be suppressed by the recombining bubbles that host most of the ionizing sources. Recovering $\bar{x}_i(z)$ will require carefully modeling this effect.

When inhomogeneous reionization is included, our models robustly predict a positive correlation between the CMB and 21 cm signals (see also Alvarez et al. 2006). This follows from the strong clustering of the first galaxies and reflects our assumption of “inside-out” reionization. An anti-correlated signal would imply that low-density gas is ionized at least as quickly as high-density gas; thus the overall sign of the correlation would provide a clean test of these contrasting approaches to reionization.

4 FOREGROUNDS AND OBSERVABILITY

There are two unavoidable sources of noise in any attempt to measure cosmic signals: the intrinsic noise associated with the detector and the error associated with sample variance (especially at low multipoles). The latter results from having only one sky and only $2\ell + 1$ independent samples at each ℓ :

$$\Delta C_{\ell}^{sv} = \sqrt{\frac{2}{(2\ell + 1)f_{\text{sky}}}} C_{\ell}, \quad (42)$$

where f_{sky} is the fraction of sky being observed. For a single 21 cm observing field this is given by $f_{\text{sky}} = d\Omega/4\pi \approx \lambda^2/(A_d 4\pi)$, approximated by the diffraction limit of the telescope, where A_d is the area of a single dish and $\lambda = 21(1 + z)$ cm.

[!t]

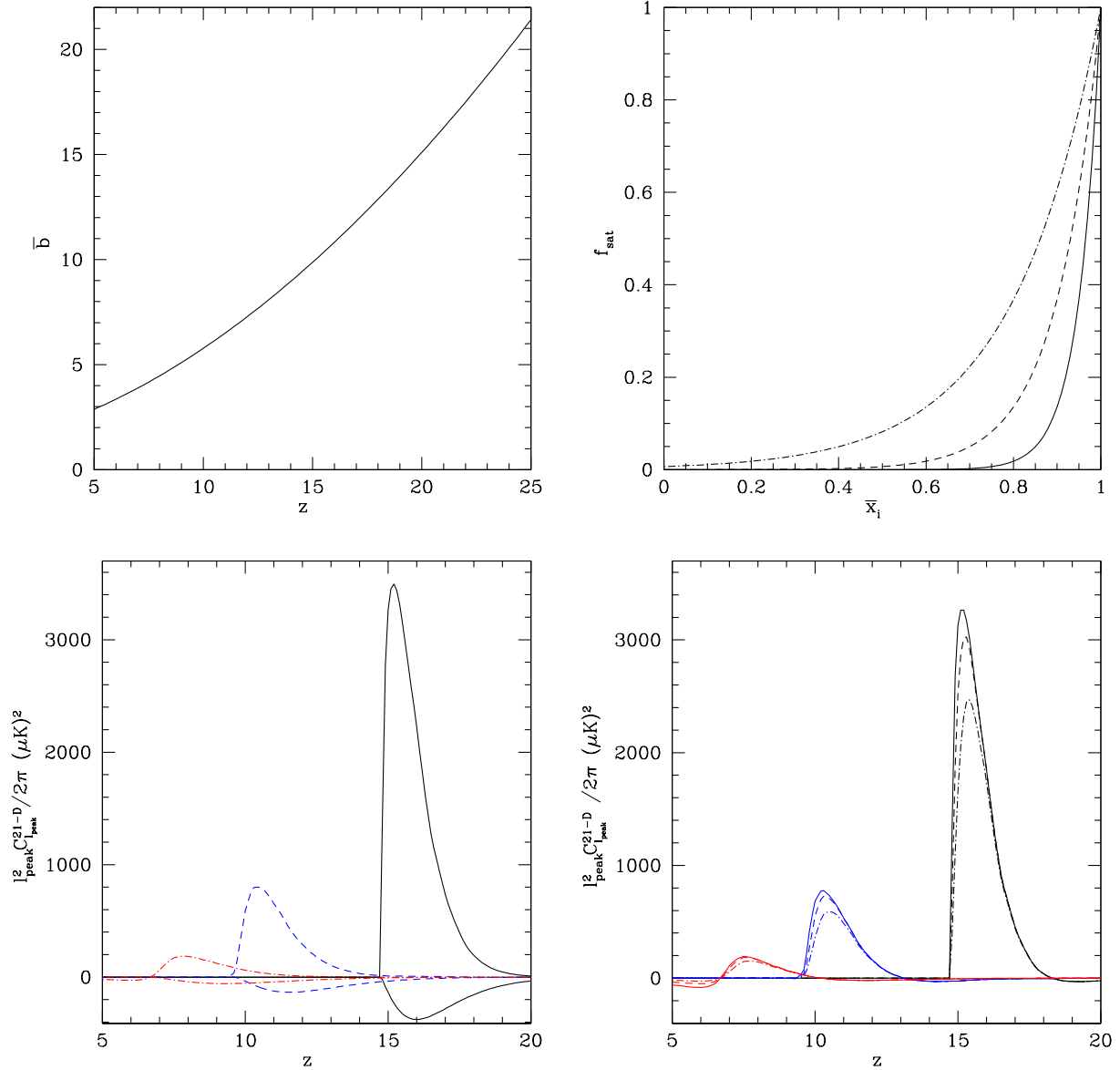


Figure 3. *Upper Left:* The mean galaxy bias function. *Upper Right:* f_{sat} for $\Delta \bar{x}_i = 0.05$ (solid curve), 0.1 (dashed curve), and 0.2 (dot-dashed curve). *Bottom left:* The homogeneous and inhomogeneous contributions to the cross correlation at ℓ_{peak} corresponding to reionization models with $\bar{x}_i=1$ at $z \approx 7, 10$ and 15 . In each case, the positive (negative) curves show the contribution from P_{δ_i} (P). All curves assume an f_{sat} with $\Delta \bar{x}_i = 0.05$. The corresponding reionization histories are shown in Fig. 2. *Bottom right:* The total signal at ℓ_{peak} . At each z , we show results for the different values of the parameter $\Delta \bar{x}_i$ in f_{sat} shown above.

While the cosmic variance contribution is purely geometric, the detector noise depends on the details of the observation. For 21 cm experiments, the RMS detector noise fluctuation per visibility of an antennae pair observing for a time t_0 in one frequency channel is (McQuinn et al. 2006)

$$\Delta V^N = \frac{\lambda^2 T_{\text{sys}}}{A_d \sqrt{\Delta \nu t_0}}, \quad (43)$$

where $T_{\text{sys}}(\nu)$ is the total system temperature. An irreducible limit on T_{sys} is provided by the radio sky itself, so $T_{\text{sys}} \geq T_{\text{sky}}$. In fact, at the low frequencies relevant to the redshifted 21 cm sky, the noise is strongly dominated by synchrotron electrons from fast electrons in the Milky Way, so to a good approximation $T_{\text{sys}} \approx T_{\text{sky}}$. A good rule of thumb for the sky temperature of high latitude, “quiet” portions of the sky is (Furlanetto et al. 2006)

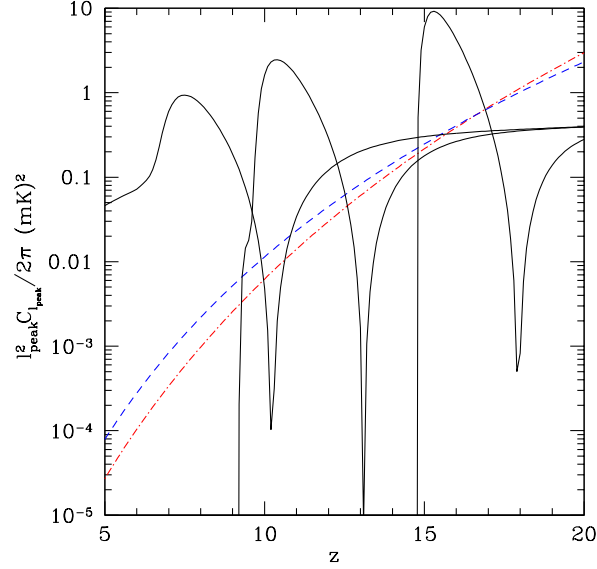


Figure 4. The thermal detector noise for 21 cm observations with the MWA (dot-dashed curve) and the SKA (dashed curve) and the intrinsic 21 cm signal for the reionization models in Fig. 2 (solid curves).

$$T_{\text{sky}} \sim 180 \left(\frac{\nu}{180 \text{ MHz}} \right)^{-2.6} \text{ K}. \quad (44)$$

It follows that the detector noise in the auto-correlation for a single baseline is

$$C_{1b}^N = \left(\frac{\lambda^2 T_{\text{sys}}}{A_d} \right)^2 \frac{1}{\Delta \nu t_0}. \quad (45)$$

The time spent observing each visibility is

$$t_{\mathbf{u}} = \frac{A_d t_0}{\lambda^2} n(\mathbf{u}), \quad (46)$$

where $u = \ell/2\pi$ and $n(\mathbf{u})$ is the average number of baselines that can observe the mode \mathbf{u} at any instant, normalized so that its integral over the \mathbf{u} plane equals the total number of baselines in the interferometer (McQuinn et al. 2006). The covariance matrix for an interferometer is then

$$C^{21,N}(\mathbf{u}) = \left(\frac{\lambda^2 T_{\text{sys}}}{A_d} \right)^2 \frac{1}{\Delta \nu t_{\mathbf{u}}}. \quad (47)$$

The total error on the autocorrelation is a combination of sample variance and detector noise

$$\Delta C_{\ell}^{21} = \sqrt{\frac{2}{(2\ell+1)f_{\text{sky}}}} \left\{ \left[\left(\frac{\lambda^2}{A_d} \right)^3 \frac{T_{\text{sys}}^2}{\Delta \nu t_0 n(\mathbf{u})} \right]^2 + (C_{\ell}^{21})^2 \right\}^{1/2}. \quad (48)$$

We estimate C_{ℓ}^{21} using equation (30) and the inhomogeneous reionization model described above; note that $P_{ii}(k) = \bar{b}^2(1 - f_{\text{sat}})^2 P(k)$ on these large scales. Figure 4 shows the intrinsic 21 cm signal for our fiducial reionization models as well as the thermal detector noise, $\ell^2 C_{\ell}^{21,N}$ for two planned experiments, the Mileura Widefield Array-Low Frequency Demonstrator (MWA) and the Square Kilometer Array (SKA). We have assumed a frequency window of $\Delta \nu = 1$ MHz, 1000 hours of observing time, and $\ell = 100$. The area of a single dish is taken to be the minimum baseline: $(4 \text{ m})^2$ for MWA and $(16 \text{ m})^2$ for the SKA, and we assume a filled core outside of which the density of antennae falls like r^{-2} . The total effective areas are 1 km^2 for the SKA and $\sim 7 \times 10^{-3} \text{ km}^2$ for the MWA.

The 21 cm signal falls sharply early in reionization because of the prefactor on the power spectrum, $[\bar{x}_{\text{HI}}(z) - \bar{b}(1 - f_{\text{sat}})\bar{x}_i(z)]^2$. These two terms cancel at a point early in reionization when the increased total density matches the decreased ionized fraction; at later times, the inhomogeneous term dominates and the signal increases again. Obviously, except when reionization occurs at $z = 15$ the intrinsic 21 cm signal significantly dominates the thermal noise. Thus any measurement of the cross-correlation is sample variance limited. Note the difference with typical 21 cm experiments, which are usually dominated by thermal noise: in this case, we are interested in such large scales that the 21 cm telescopes can measure the modes in detail at least neglecting foreground contamination). We neglect the 21 cm detector noise for the remainder of the paper.

For the CMB, experiments like *WMAP* are already nearly signal-variance limited on scales near ℓ_{peak} . Thus we neglect the thermal noise term entirely for the CMB.

One of the general advantages of cross correlation is that any uncorrelated noise (such as the thermal noise in each detector) will vanish. Unfortunately, many of the strong foregrounds for 21 cm observations also appear at CMB frequencies (such as the Galactic synchrotron radiation and radio point sources). However, we will assume optimistically that cleaning of the separate maps will effectively remove this contamination (Zaldarriaga et al. 2004; Morales & Hewitt 2004; Santos et al. 2003; Morales et al. 2006; McQuinn et al. 2006); in reality, foregrounds could make the signal even more difficult to detect than estimated here.

We can then estimate the $1\text{-}\sigma$ error for the cross-power spectrum from

$$(\Delta C_\ell^{21-D})^2 \approx \frac{1}{(2\ell+1)f_{\text{sky}}\Delta\ell} [(C_\ell^{21-D})^2 + C_\ell^{CMB}C_\ell^{21}], \quad (49)$$

where $\Delta\ell$ is the size of the bins over which the power spectrum is averaged ($\ell - \Delta\ell/2 < \ell < \ell + \Delta\ell/2$). In terms of the cross-correlation coefficient, the expected fractional error (eq. 49) can be written:²

$$\frac{\Delta C_\ell^{21-D}}{C_\ell^{21-D}} = \frac{1}{\sqrt{(2\ell+1)f_{\text{sky}}\Delta\ell}} \frac{\sqrt{1+r^2}}{r}. \quad (50)$$

This result has a simple physical interpretation. The first factor on the right hand side is the fractional error from cosmic variance for any autocorrelation. If the two signals are weakly correlated, $r \ll 1$, only a portion of each intrinsic signal is useful for the measurement and the cosmic variance limit increases accordingly. This can be recast as a constraint on the minimum correlation coefficient r observable with a given signal-to-noise on the cross-power:

$$r > \left[\left(\frac{\Delta C_\ell^{21-D}}{C_\ell^{21-D}} \right)^2 (2\ell+1)f_{\text{sky}}\Delta\ell - 1 \right]^{-1/2}. \quad (51)$$

Thus the observability of our signal will depend on the cross-correlation coefficient. We can estimate its value by comparing equation (32) for our reionization models to the total primordial CMB anisotropies. For the models in Figure 2, we find $\ell^2 C_\ell^{DD}/2\pi = 19.8 \mu\text{K}^2$, $2.4 \mu\text{K}^2$, and $0.4 \mu\text{K}^2$ for the $z = 15$, $z = 10$, and $z = 7$ cases respectively. The primary anisotropy is $\approx (40 \mu\text{K})^2$ at $\ell = 100$, so even if the Doppler component of the CMB is completely correlated with the 21 cm signal (see below), we must still have $r < 0.11$, 0.04 and 0.015 for the $z = 15$, 10 and 7 cases, respectively. One can already see that the prospects for detecting the cross-correlation are dim: the CMB at $\ell \approx 100$ is well-fit by the primary anisotropies alone, ignoring the Doppler terms from reionization, and has been observed to nearly the cosmic variance limit (Spergel et al. 2006). The fractional cosmic variance errors for C_ℓ^{21-D} will be larger than those on the CMB by a factor $1/r$.

For a concrete (though optimistic) estimate, let us assume that we have $f_{\text{sky}} = 1/2$ and sum over all multipoles. Thus we forsake any shape information in order to test the null hypothesis, that is, whether or not correlation can be distinguished from no correlation. For this calculation, we assume for simplicity that the correlation coefficient between the Doppler anisotropy and the 21 cm brightness, $r_{21-D} = r\sqrt{C_\ell^{CMB}/C_\ell^{21-D}}$, is independent of scale and we choose the observed frequency to correspond to the peak of the cross-correlation. We can then find the total signal to noise ratio from (compare eq. 51 of Slosar et al. 2007)

$$SNR^2 = \sum_\ell \left(\frac{C_\ell^{21-D}}{\Delta C_\ell^{21-D}} \right)^2 \approx r_{21-D}^2 \sum_\ell (2\ell+1)f_{\text{sky}} \frac{C_\ell^{DD}}{C_\ell^{cmb}}, \quad (52)$$

since C_ℓ^{DD}/C_ℓ^{cmb} is small. We find signal to noise ratios of $SNR \sim 2 r_{21-D}$, $5 r_{21-D}$, and $14 r_{21-D}$ for reionization ending at $z = 7$, 10 , and 15 , respectively. If the 21 cm signal and the Doppler signal were perfectly correlated, then we could conceivably detect the correlation in all these scenarios. However, in reality the correlation coefficient between the 21 cm signal and the Doppler signal is $r_{21-D} \sim 0.3$. Thus it is unlikely that we can detect the cross-correlation if reionization ends at $z \lesssim 12$. For reionization at higher redshifts, a detection is possible provided we can view $\gtrsim 50\%$ of the sky.

Of course, the above estimate assumes a single frequency band for the 21 cm map; increasing the frequency coverage will provide more samples and improve the total signal-to-noise (though at the cost of losing any information about the signal's evolution with redshift). However, $\ell \sim 100$ corresponds to 200 Mpc. Demanding that each 21 cm frequency slice be statistically independent then requires that the slices be ~ 10 MHz thick, which corresponds to $\Delta z \sim 1$. Thus there are in fact relatively few independent slices available, unless reionization is considerably more extended than in our simple models (in which case each individual slice would have a smaller signal anyway).

5 DISCUSSION AND CONCLUSION

In this work we have calculated the large scale cross correlation between the CMB temperature anisotropy and the 21 cm background, improving the calculation of Alvarez et al. (2006). The signal is expected to come from large angular scales ($\ell \sim 100$) corresponding to

² Note that our definition of the cross-correlation coefficient r ignores the noise terms.

~ 200 Mpc at redshifts $z \sim 10$. On these scales linear theory is still valid, which greatly simplifies the analysis. We have also presented a new model for the evolution of the ionized contrast as reionization proceeds that includes the effects of recombinations in limiting the apparent bias of reionized regions.

The cross correlation arises from the connection between linear overdensities and the baryon velocity field via the continuity equation in linear theory. Fluctuations in the underlying density field source brightness fluctuations in the 21 cm background, while the baryon velocity field Doppler scatters the CMB. The evolving ionized fraction, which is analogous to the evolving gravitational potentials in the integrated Sachs-Wolfe effect, reduces the line of sight cancellation that is usually associated with Doppler contributions to secondary anisotropies. Moreover, the redshift information contained in the 21 cm signal (as a binning in frequency) allows us to reconstruct 3D information about the cross correlation.

Our calculations include improvements to the approach originally presented by Alvarez et al. (2006). The key differences are the treatment of the bulk velocity corrections to the 21 cm signal, the reionization model, and the ionized fraction-density cross-correlation.

Alvarez et al. (2006) chose a particular functional form $\ln[1 - \bar{x}_i] = -\zeta_0(z)f_{\text{coll}}(z)$ for the reionization history. Although it is driven by the same mechanism as ours early in reionization (the time evolution of f_{coll}), this form demands that the reionization history slow when $\bar{x}_i > 0.5$. Although such a delay can be loosely attributed to either feedback or recombinations, there is in fact no requirement that they set in so early, or that they slow the subsequent evolution so dramatically.

Our model, on the other hand, explicitly relates the collapsed fraction to the ionized fraction, to which we add the effects of recombinations (which limit the bubble sizes and mediate the source bias). Following Furlanetto & Oh (2005), we assume that ionized bubbles grow until they reach a size R_{max} , where recombinations prevent subsequent growth. Any more ionizing photons produced in these bubbles are canceled out by recombinations. As reionization proceeds more and more bubbles saturate and no longer contribute to the global evolution of the ionized fraction. As this process unfolds, more of the collapsed matter enters these saturated bubbles, so the ionized contrast between over- and underdense regions begins to get smaller, eventually shrinking to zero as all regions become ionized.

These differences change the amplitude and evolution of the signal but not its qualitative behavior. Like Alvarez et al. (2006), in the case of homogeneous reionization we find an anti-correlation between the 21 cm signal and the CMB. In this case an overdensity simultaneously increases the brightness of the 21 cm background and cools the CMB through Thomson scattering across regions where x_i is increasing. The contribution from the homogeneous term decreases with redshift due to dilution of the matter density through Hubble expansion.

The result is markedly different when inhomogeneous reionization is included: the 21 cm and CMB signals become strongly correlated. Ionized clumps still scatter and cool the CMB photons through the x_i gradient. However, these regions also cause a significant *negative* fluctuation in the 21 cm brightness due to the large deficit of neutral hydrogen. This term is strongly boosted by the galaxy bias and dominates over the anti-correlated homogeneous reionization contribution.

Of course, this positive correlation rests on our assumption that reionization proceeds inside-out. If instead low density gas is ionized first, the inhomogeneous component would become anti-correlated: the underdense regions would blueshift the CMB photons while decreasing the 21 cm brightness both through a decreased matter density and ionized fraction.

Unfortunately, we have shown above that the 21 cm and CMB signals are too weakly correlated for the cross-correlation to be easily detectable. Like Alvarez et al. (2006), we find that thermal noise will not pose a significant problem because the correlation only appears on large scales, where 21 cm telescopes are sample variance-limited. However, when we include cosmic variance of the 21 cm signal, the prospects for detection look dim. The cross-correlation coefficient between the total CMB signal and the 21 cm background is only $r \lesssim 0.03$: it is small because the Doppler contribution makes up $\lesssim 1\%$ of the total CMB anisotropy, and only $\sim 30\%$ of that correlates with the 21 cm background. Experiments targeting this signal will require extremely large fields of view, and even then will be unable to recover the signal at high signal-to-noise or to trace its angular power spectrum. Prospects are actually best for early reionization, because then the CMB Doppler term is increased by the denser gas during reionization. (Note also that we have ignored foreground contamination in the 21 cm signal, which must be cleaned and will further degrade the detectability.)

Although it is possible that our models under-predict the cross-correlation signal, our predictions for the detectability is robust. We have shown that the signal to noise ratio is limited primarily by the smallness of the Doppler signal. The size of the Doppler contributions is determined entirely by the rate of reionization and the epoch at which reionization occurs. Our models already provide relatively fast reionization, so the signal can probably only be increased in this fashion by a factor of ~ 2 , which does not change our conclusions. Furthermore, while detection of the cross-correlation at $\ell \sim 100$ is limited by the cosmic variance of the 21 cm and CMB signals, it does not help to move to higher multipoles where there are more modes available. On the one hand, moving to higher ℓ may increase the effective bias, $\bar{b}(z)$, and thus the cross-correlation, as the scale approaches the characteristic bubble size. However, this aspect would only boost the 21 cm signal (which does not help much because it also increases the cosmic variance) and not the Doppler signal. In fact, as shown by Giannantonio & Crittenden (2007) the Doppler signal, and hence the ratio C_ℓ^{DD}/C_ℓ^{CMB} , begins to sharply decrease after $\ell \sim 100$: any gains made in sampling more modes are immediately lost.

We thank M. Zaldarriaga and M. Alvarez for helpful comments on the manuscript and A. Mesinger for sharing simulation data with us.

REFERENCES

Alvarez M. A., Komatsu E., Dore O., Shapiro P. R., 2006, *Astrophys. J.*, 647, 840

- Barkana R., Loeb A., 2001, Phys. Rept., 349, 125
 Barkana R., Loeb A., 2005, Astrophys. J., 624, L65
 Bharadwaj S., Ali S. S., 2004, Mon. Not. Roy. Astron. Soc., 352, 142
 Cen R., 2003, ApJ, 591, 12
 Ciardi B., Madau P., 2003, ApJ, 596, 1
 Cooray A., 2004, Phys. Rev., D70, 063509
 Dodelson S., Jubas J. M., 1995, ApJ, 439, 503
 Eisenstein D. J., Hu W., 1997, Astrophys. J., 511, 5
 Fan X., et al., 2002, AJ, 123, 1247
 Fan X., et al., 2006, AJ, 132, 117
 Fan X.-H., Carilli C. L., Keating B., 2006, Ann. Rev. Astron. Astrophys., 44, 415
 Field G. B., 1958, Proceedings of the Institute of Radio Engineers, 46, 240
 Furlanetto S., 2006, Mon. Not. Roy. Astron. Soc., 371, 867
 Furlanetto S. R., Loeb A., 2005, Astrophys. J., 634, 1
 Furlanetto S. R., Oh S. P., 2005, Mon. Not. Roy. Astron. Soc., 363, 1031
 Furlanetto S. R., Oh S. P., Briggs F., 2006, Phys. Rept., 433, 181
 Furlanetto S. R., Zaldarriaga M., Hernquist L., 2004a, Astrophys. J., 613, 1
 Furlanetto S. R., Zaldarriaga M., Hernquist L., 2004b, Astrophys. J., 613, 16
 Giannantonio T., Crittenden R., 2007
 Holder G. P., Haiman Z., Kaplinghat M., Knox L., 2003, ApJ, 595, 13
 Hu W., 1996, Lect. Notes Phys., 470, 207
 Hu W., Scott D., Silk J., 1994, PRD, 49, 648
 Kaiser N., 1987, Mon. Not. Roy. Astron. Soc., 227, 1
 Lewis A., Challinor A., 2007
 McQuinn M., Furlanetto S. R., Hernquist L., Zahn O., Zaldarriaga M., 2005, Astrophys. J., 630, 643
 McQuinn M., Zahn O., Zaldarriaga M., Hernquist L., Furlanetto S. R., 2006, Astrophys. J., 653, 815
 Madau P., Meiksin A., Rees M. J., 1997, ApJ, 475, 429
 Mesinger A., Furlanetto S., 2007
 Miralda-Escude J., Haehnelt M., Rees M. J., 2000, Astrophys. J., 530, 1
 Mo H. J., White S. D. M., 1996, Mon. Not. Roy. Astron. Soc., 282, 347
 Morales M. F., Bowman J. D., Hewitt J. N., 2006, ApJ, 648, 767
 Morales M. F., Hewitt J., 2004, ApJ, 615, 7
 Mortonson M. J., Hu W., 2007, ApJ, submitted (arXiv.org/0705.1132 [astro-ph]), 705
 Page L., et al., 2007, ApJS, 170, 335
 Press W. H., Schechter P., 1974, Astrophys. J., 187, 425
 Salvaterra R., Ciardi B., Ferrara A., Baccigalupi C., 2005, Mon. Not. Roy. Astron. Soc., 360, 1055
 Santos M. G., Cooray A., Haiman Z., Knox L., Ma C., 2003, ApJ, 598, 756
 Scott D., Rees M. J., 1990, MNRAS, 247, 510
 Shaver P. A., Windhorst R. A., Madau P., de Bruyn A. G., 1999, A&A, 345, 380
 Slosar A., Cooray A., Silk J., 2007
 Spergel D. N., et al., 2006
 White R. L., Becker R. H., Fan X., Strauss M. A., 2003, AJ, 126, 1
 Wyithe J. S. B., Loeb A., 2003, ApJ, 588, L69
 Zaldarriaga M., 1997, PRD, 55, 1822
 Zaldarriaga M., Furlanetto S. R., Hernquist L., 2004, Astrophys. J., 608, 622

APPENDIX A: INTEGRAL APPROXIMATION

Consider the integral representation of the 3D Dirac delta function,

$$(2\pi)^3 \delta(\mathbf{r} - \mathbf{r}') = \int d^3k \exp[i\mathbf{k} \cdot (\mathbf{r} - \mathbf{r}')]. \quad (\text{A1})$$

Expanding the plane wave in spherical coordinates, we obtain

$$(2\pi)^3 \delta(\mathbf{r} - \mathbf{r}') = (4\pi)^2 \int d^3k \sum_{\ell, m} (-i)^\ell j_\ell(kr) Y_{\ell m}(\hat{\mathbf{k}}) Y_{\ell m}^*(\hat{\mathbf{r}}) \sum_{\ell', m'} (i)^{\ell'} j_{\ell'}(kr') Y_{\ell' m'}^*(\hat{\mathbf{k}}) Y_{\ell' m'}(\hat{\mathbf{r}}') \quad (\text{A2})$$

$$= (4\pi)^2 \sum_{\ell, m} \int k^2 dk j_\ell(kr) j_\ell(kr') Y_{\ell m}(\hat{\mathbf{r}}) Y_{\ell m}^*(\hat{\mathbf{r}}'), \quad (\text{A3})$$

where we have used the orthogonality of the spherical harmonics. Now in spherical coordinates we can express the Dirac delta function as

$$\delta(\mathbf{r} - \mathbf{r}') = \delta(\Omega, \Omega') \frac{\delta(r - r')}{r^2}, \quad (\text{A4})$$

so that multiplying equation (A3) by $Y_{\ell m}(\hat{\mathbf{r}}')$ and integrating over $d\Omega'$ yields

$$\int_0^\infty k^2 dk j_\ell(kr) j_\ell(kr') = \frac{\pi}{2} \frac{\delta(r-r')}{r^2}. \quad (\text{A5})$$

In this paper we encounter an integral similar to the left hand side of equation (A5), but with another smooth function of k , $P(k)/k^2$, in the integrand. The spherical Bessel functions $j_\ell(kx)$ are very small for $kx < \ell$ and start to oscillate for $kx \sim \ell$. As can be seen from (A5), the Bessel functions are out of phase for any separation of the points r and r' . The integral will thus only receive contributions from a region around the first peak, which occurs at $k \sim \ell/x$. We then make the approximation $P(k) \approx P(k = \ell/r)$ (e.g., Zaldarriaga et al. 2004), and pull it out of the integral to obtain the approximation used in the main body of the paper:

$$\frac{2}{\pi} \int_0^\infty k^2 dk \frac{P(k)}{k^2} j_\ell(kr) j_\ell(kr') \approx P\left(k = \frac{\ell}{r}\right) \frac{\delta(r-r')}{\ell^2}. \quad (\text{A6})$$